Production of Immunoabsorbent Nanoparticles by Displaying Single-Domain Protein A on Potato Virus X[a]

Kerstin Uhde-Holzem, Michael McBurney, Brylee David B. Tiu, Rigoberto C. Advincula, Rainer Fischer, Ulrich Commandeur,* Nicole F. Steinmetz*

The combination of antibodies with nanoparticles provides wide-ranging applications in biosensing. While several covalent presentation strategies have been established, there is need for alternative, non-covalent methods to provide a routine for scalable nanomanufacturing. We report the multivalent presentation of the B domain of *Staphylococcus aureus* protein A (SpAB) on potato virus X (PVX) nanoparticles. Three different synthetic strategies were used to obtain chimeric PVX^{SpAB} filaments. The protein A fragments displayed on the surface of all three PVX chimeras remained fully functional as an immunoabsorbent for antibody capture enabling biosensing. The new biomaterials presented could find applications as diagnostic tools for biomedical or environmental monitoring.

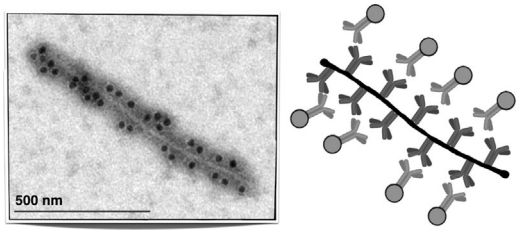

1. Introduction

Antibodies and their conjugates find applications across scientific disciplines and are applied in research, development, and industry. The combination of antibodies with nanoparticles provides a means for multifunctional and multiplexed systems; and the combination of these systems with nanomanufacturing techniques enables the production of miniaturized devices with enhanced sensing capabilities. Several covalent strategies for antibody display have been developed, most of which rely on chemical conjugation. Traditional approaches include coupling between nanoparticle and antibody through the formation of amide bonds, stable imines, or isourea derivatives.

U. Commandeur, K. Uhde-Holzem, R. Fischer
Institute for Molecular Biotechnology, RWTH Aachen University, Worringer Weg 1, 52074 Aachen, Germany
E-mail: commandeur@molbiotech.rwth-aachen.de
N. F. Steinmetz, M. McBurney
Department of Biomedical Engineering, Case Western Reserve University Schools of Medicine and Engineering, Cleveland, Ohio 44106, USA
E-mail: nicole.steinmetz@case.edu
R. Fischer
Fraunhofer Institute for Molecular Biology and Applied Ecology IME, Forckenbeckstraße 6, 52074, Aachen, Germany

N. F. Steinmetz, B. D. B. Tiu, R. C. Advincula
Department of Macromolecular Science and Engineering, Case Western Reserve University Schools of Medicine and Engineering, Cleveland, Ohio 44106, USA
N. F. Steinmetz
Department of Radiology, Case Western Reserve University Schools of Medicine and Engineering, Cleveland, Ohio 44106, USA
N. F. Steinmetz
Department of Materials Science and Engineering, Case Western Reserve University Schools of Medicine and Engineering, Cleveland, Ohio 44106, USA

[a]**Supporting Information** is available from the Wiley Online Library or from the author.

DOI: 10.1002/mabi.201500280

The latter requires chemical modification of the antibody, which potentially alters and/or interferes with its target specificity.[1–4] Harsh chemical reaction conditions may denature the antibody; some reactions require multiple steps and, therefore, may be low yielding; and most reactions do not provide orientational control over antibody presentation. Therefore, alternative strategies for stable and scalable manufacturing of antibody–nanoparticle conjugates need to be devised. Striving for this goal, we turned toward a bio-inspired nanoparticle platform technology with engineered antibody capture strategy.

Nanoparticles are an emerging tool for biomedical applications, and many nanoparticle–antibody conjugates are in development for diverse applications. While synthetic nanoparticles can harbor interesting physiochemical properties, such as the fluorescent probes derived from quantum dots, bio-derived nanoparticles offer several advantages: bionanoparticles are generally nontoxic, biodegradable, and biocompatible. Protein-based nanoparticles are of particular interest because they are inherently compatible for antibody presentation; protein denaturation and spreading of proteins on synthetic nanoparticles.[5]

In this study, we turned toward the flexible filaments formed by the potato virus X (PVX) as a platform technology for antibody presentation. Potato virus X, the type member of the Potexvirus group is a monopartite plant virus.[6] Its particles are filamentous and flexible rods 515 nm in length and 13 nm wide comprising 1270 identical 25 kDa coat protein (CP) subunits. The *N*-terminal part of the CP is thought to be solvent-exposed; however, the crystal structure of PVX has not been solved, yet. Therefore, most coat protein fusions reported are based on *N*-terminal fusions.[7–9] It should be noted that *C*-terminal PVX coat protein fusions of peptides and proteins have also been reported.[10,11] In addition to the genetic engineering capabilities, chemical modification enables additional functionalization post-harvest. We established bioconjugation protocols targeting surface-exposed lysines using *N*-hydroxysuccinimide or Cu(I)-catalyzed azide–alkyne cycloaddition (click chemistry) enabling efficient functionalization of PVX with biotin linkers, fluorophores, PEG, targeting ligands, etc.[12–15]

To date PVX has been used for epitope presentation approaches in vaccine development;[9,16] chimeric PVX particles have also been combined with enzymes for the fabrication of novel biocatalysts,[17] and PVX is undergoing development as a novel carrier for oncological imaging and therapeutic intervention.[12–15] To extend the application of PVX, we set out to combine the platform technology with protein A fragments for functionalization for antibodies. The potential application of such antibody-functionalized filaments is envisioned in medical imaging or drug delivery when combined with contrast agents and or toxic payloads as well as in diagnostics; the latter was investigated in the present study.

To enable non-covalent antibody display with orientational control, we used a synthetic biology approach to present protein A fragments on the PVX-based nanoparticle. In nature, the Protein A is found exposed on the cell surface of the gram-positive bacterium *Staphylococcus aureus*. It is composed of a 42-kDa single polypeptide chain, folded into five highly homologous domains, termed E, D, A, B, and C, each composed of 56–61 residues. Its special interest in biotechnology is due to three prominent properties: 1. Its structural stability over a broad range of pH levels (pH 2-12) and in the presence of various detergents; 2. The IgG–protein A complex interaction is reversible; while stable over a broad range of physiological conditions, dissociation is possible under controlled conditions (pH 3.5–4.5) without apparent loss of activity. 3. Its reversible binding of a large variety of IgGs through the consensus sequence (Asn–Gln–Phe–Asn–Lys–Glu) of the Fc fragment. Protein A exhibits high affinity to human, rabbit, and guinea pig IgGs, offering a platform technology for combination with a diverse set of target antibodies. Since protein A detects the Fc portion of IgGs,[18] it is expected to enable a controlled Fc site-specific antibody immobilization on PVX particles resulting in a target-directed Fab presentation.

We describe the fusion of the PVX coat protein (CP) with protein A (SpAB) fragments using genetic engineering; three distinct display strategies were investigated; each of which yielded functional PVX^{SpAB}CP filaments enabling efficient antibody capture and presentation. As a proof-of-concept, we tested the integration of PVX^{SpAB}CP particles in sensing applications: PVX^{SpAB}CP was immobilized on gold chips and implemented as virus sensor using quartz crystal microbalance detection.

2. Results and Discussion

The fusion of the protein A domain B (referred to as SpAB) to the *N*-terminus of the PVX coat protein was accomplished in three different ways: (i) SpAB was fused directly to the *N*-terminus of the PVX CP, (ii) SpAB was fused to the *N*-terminus of the PVX CP via a flexible glycine-rich $(G_4S)_3$ linker (G4S), and (iii) SpAB was fused to the *N*-terminus of PVX CP via an intervening foot and mouth disease virus (FMDV) 2A sequence, which mediates co-expression of free CP and SpAB-Cp fusion protein (Figure 1). Some investigations indicated that direct fusion of polypeptides to the PVX CP requires presence of wild-type CP to facilitate assembly of the filamentous particles. This so-called ''overcoat principle'' is achieved when the 2A sequence is inserted between the foreign and the coat protein sequence as a translational fusion; the 2A sequence induces a

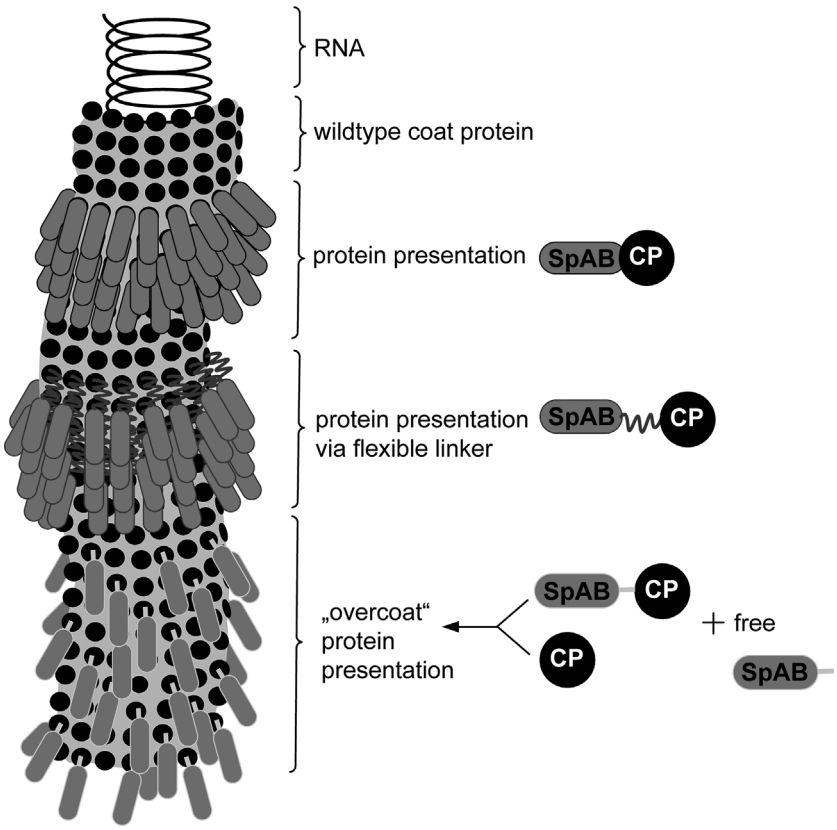

Figure 1. Schematic drawing of chimeric PVX particles.

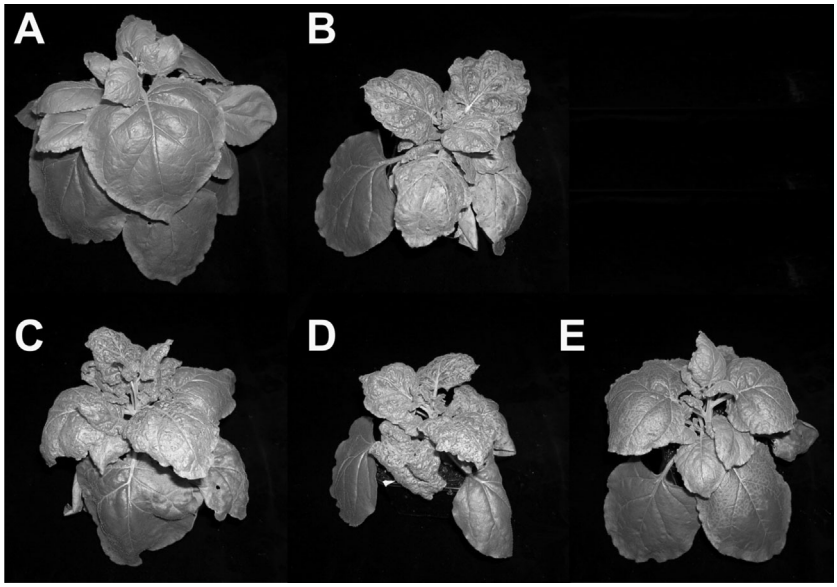

Figure 2. *N. benthamiana* plants (6 weeks after seeding). (A) Healthy *N. benthamiana* plant. (B–E) *N. benthamiana* plants 13 d post inoculation (dpi). DNA plasmids used for inoculation: (B) PVX201 (wild-type PVX), (C) $PVX^{SpAB}CP$ (direct SpAB-CP fusion), (D) $PVX^{SpAB\text{-}2A}CP$ (fusion via 2A sequence SpAB-2A-CP), (E) $PVX^{SpAB\text{-}G4S}CP$ (fusion via glycine linker SpAB-G4S–CP). (See also Supporting Figure S1.)

ribosomal skip leading to co-expression of free CP and fusion CP. The use of the 2A sequence has been proven successful for insertion of large polypeptide sequences into the PVX CP, e.g., 238-amino-acid-long green fluorescent protein (GFP).[19] In our studies, we set out to systematically investigate whether the insertion of a linker sequence was required, therefore expression constructs with and without 2A and $(G_4S)_3$ linkers were designed and evaluated.

Three to four days after inoculation of *N. benthamiana* plants with plasmid DNA containing the chimeric PVX genome, local and systemic infection was notable for all three constructs. Two weeks after inoculation, systemic infection extended over the whole plant (Figure 2 and Supporting Figure S1). Before scaled-up nanomanufacturing was initiated, the genetic, protein-chemical, and structural integrity of the constructs were verified using crude plant sap and SDS PAGE (not shown), Western Blot analysis (Figure 3), and electron microscopy (Figure 4).

Western Blot analysis of the crude extract prepared from these leaves revealed that plant sap from plants contained high level of the fusion protein, with a strong prominent band corresponding to their theoretical molecular weight of 31.6 kDa ($PVX^{SpAB}CP$), 33.7 kDa $PVX^{SpAB\text{-}2A}CP$, and 32.7 kDa ($PVX^{SpAB\text{-}G4S}CP$) (Figure 3). In addition for all PVX constructs CP dimer bands as well as unknown CP degradation products were observed. This is a phenomenon already described earlier for PVX CP fusion proteins such as PVX-R9.[9] For $PVX^{SpAB\text{-}2A}CP$ (see Figure 3, lanes 4–7) besides the prominent band at 33.7 kD a faint band can be observed for the free wild-type CP at 25 kD.

To determine whether the three different protein A CP fusions also assembled into viral particles, crude extracts were analyzed using the electron microscope (Figure 4). Microscopy confirmed that in all three configurations, virus particles of filamentous nature were produced. Particles appearance was similar to wild-type particles; however, it was noted that chimeric particles differed from the wild-type particles by stronger adsorption to

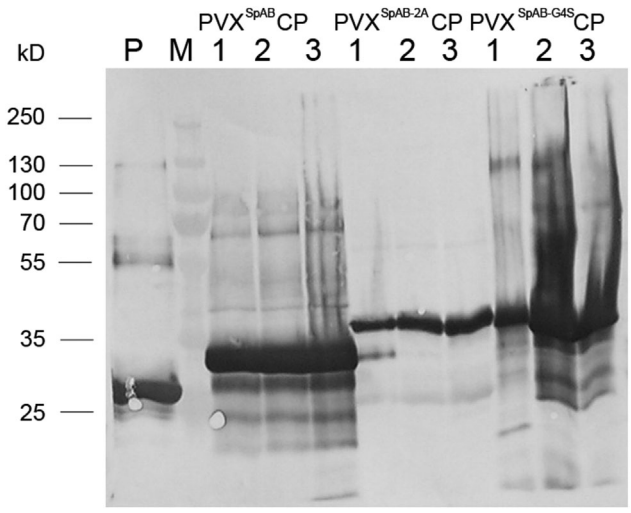

Figure 3. Western blot analysis of PVX^{SpAB} proteins from systemically infected *N. benthamiana* plant leaves 13 dpi. Leave extracts were diluted 1:3 in PBS, PVX^{SpAB}CP (1–3) and PVX$^{SpAB\text{-}2A}$CP (4–6) and PVX$^{SpAB\text{-}G4S}$G4S (7–9). Lane designations: M = prestained broad range marker SM1811 (Fermentas); P = PVX^{wt}CP control; 1–3, 4–6, and 7–9: three different PVX infected plants, respectively. Antibody detection: pAb PVX (1:2000) and GAR^{AP} (1:5000).

the grid and/or more intense staining, reflected by higher electron density surrounding the particles.

Next, we investigated whether the functional domain of SpAB was conserved when presented on the PVX nanofilament: capture and presentation of antibodies to the protein A-displaying PVX particles was first investigated using immunogold labeling and electron microscopy (Figure 4). It is known that protein A binds efficiently to the constant regions of many subclasses of IgG from different species.[20] Here, we tested either the direct capture of gold-conjugated antibody (from rabbit) or the indirect capture, using a primary unlabeled antibody (human 2G12) and a secondary gold-conjugated antibody (GAH^{15nm}) (Figure 4). Either approach resulted in PVX^{SpAB}CP nanoparticles heavily decorated with gold nanoparticles over the entire length of the filaments, indicating uniform antibody capture and display. Somewhat surprisingly, we also observed unstained PVX particles, i.e., free of gold-labeled antibodies, in all three samples. This may indicate presence of wild-type PVX—potentially through loss of the gene of interest due to homologous or heterologous recombination events. It is also possible that the protein A displayed on the particles lost structural or functional properties over extended storage. In fact, it has been reported that protein A expressed in altered microenvironments may be inherently less stable.[21] Nevertheless, this instability can be overcome through storage at −20 °C or by adding protease inhibitors (2 mM EDTA and 1 mM PMSF).

Therefore, for future application and potential commercialization of the PVX platform as immunosorbent nanoparticles, further research is required to investigate the stability in more detail: it will be critical to address at which level instability occurs. If genetic instability is indicated, we will consider the development of agrobacterium-based expression strategies. Expression of virus-like particles in plants through agroinoculation has been proven a valid production strategy facilitating scaled-up manufacture; for example, Medicago, Inc. already produces a large product line of virus-like particles in plants. If instability occurs during storage, we could explore alternative linker strategies or stabilize the construct through mild cross-linking post harvest. Further, we recommend to prepare fresh batches of particles and store products at −20 °C. In addition, RT-PCR and immunogold transmission electron microscopy analysis are recommended prior implementation into devices. Using DNA-based expression constructs, we achieved nanomanufacturing of protein A-displaying PVX^{SpAB}CP particles at the milligram scale. Structurally and functionally sound particles were recovered at yields of 100 mg kg^{-1} of leaf biomass. Future optimization of the expression constructs and strategy is expected to increase the yields even further.

Antibody–PVX^{SpAB}CP interactions were probed using dot blot tests; PVX^{SpAB}CP and controls (PBS or PVX) were immobilized onto nitrocellulose membranes and probed with total human IgG, total rabbit IgG, rabbit anti-CPMV protein G purified serum, and rabbit anti-prostate specific antigen (PSA) antibodies followed by detection using alkaline phosphatase-labeled secondary antibodies. Dot blot tests indicate successful interaction of PVX^{SpAB}CP with the target antibody (Figure 5). Non-specific interactions with native PVX or non-specific adsorption onto the membranes of any of the antibodies studied were not apparent.

Next, we evaluated antibody-to-PVX^{SpAB}CP binding using quartz crystal microbalance with dissipation monitoring (QCM-D). PVX^{SpAB}CP was immobilized by adsorption onto a gold sensor chip (native PVX or PBS were used as controls); then antibodies of interest were subjected to the functionalized sensor chip surfaces (Figure 6, Table 1). Direct immobilization experiments indicate non-specific adsorption of the antibodies onto the gold sensor chips. This is a common phenomenon; proteins, including antibodies, bind non-specifically onto synthetic surfaces such as gold; in some cases this non-specific adsorption can lead to spreading and denaturing of the protein,[5] therefore underlying the need for biocompatible immobilization techniques. The deposition of total human IgG directly onto the gold surface and its deposition onto a PVX-functionalized gold sensor chip followed the same trend. Recorded changes in frequency were at Δf −29.3 Hz and Δf −30 Hz in either experiment; this was accompanied

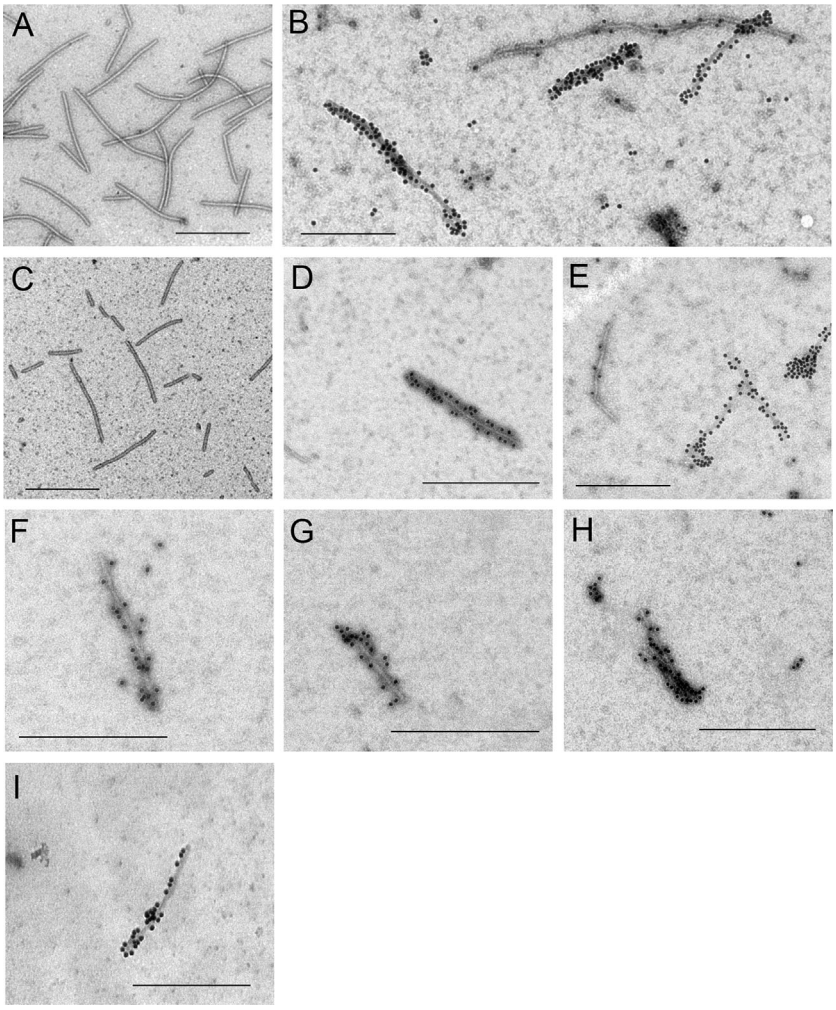

Figure 4. Electron microscopy of wild-type PVX (PVX201) and PVX^{SpAB}CP particles. (A, C) wild-type PVX (PVX201) particles, (B, D, E) PVX^{SpAB}CP particles. (F, G, H) PVX$^{SpAB\text{-}G4S}$CP particles, (I) PVX$^{SpAB\text{-}2A}$CP particles. (A + B) Detection with human 2G12 antibody (1 μg mL^{-1}) 1:1000 and 15 nm gold labeled GAH antibody. (C–I) 15 nm gold labeled GAR antibody. Bars = 500 nm.

by comparatively small dissipation shifts of about ΔD -0.8×10^{-6} and 2.13×10^{-6} indicating rigid immobilization of the antibodies. When studying the PVX^{SpAB}CP-functionalized surface, it was apparent that a significantly larger amount of total human IgG could be captured, the change in frequency of $\Delta f = 55.3$ Hz was accompanied with a small change in dissipation $\Delta D = 0.2 \times 10^{-6}$, again indicating rigid and stable immobilization. The antibodies were stably and irreversibly bound, with no desorption being observed when the solution was replaced by buffer.

The reported changes in frequency Δf are directly correlated to the mass (Δm) deposited on the sensor surface; therefore, we can conclude that approximately twice the amount of human total IgG was deposited onto the PVX^{SpAB}CP-functionalized sensor compared to non- or PVX-functionalized sensors. The deposited mass (Δm) can be calculated: a small mass deposited on the sensing surface of the quartz crystal will cause a decrease in Δf, which is proportional to Δm if (i) the mass is small compared to the mass of the crystal, (ii) is distributed evenly, (iii) does not slip on the surface, and (iv) is sufficiently rigid and/or thin to have negligible internal friction. In this case, the Sauerbrey equation[22] applies:

$$\Delta m = -C\Delta f/n$$

where C is the sensitivity constant ($C = 17.7$ ng cm^{-2} Hz^{-1} for a 5 MHz crystal) and n is the overtone with $n = 1$, 3, 5,...

Considered the negligible changes in ΔD and based on the assumption that points i–iv apply, Δm deposited for PVX and the subsequent antibody layer were calculated (Table 1). It was interesting to note that native PVX showed stronger adsorption onto the gold sensor chip compared to the engineered PVX^{SpAB}CP. While 158.4 ng PVX^{SpAB}CP were deposited onto the surface, approximately twice the amounts of PVX were immobilized (296.7 ng). This may be explained by the different surface properties: While native PVX has an isoelectric point of pI ≈ 6.7, the chimeric PVX^{SpAB}CP has a more acidic isoelectric point with pI ≈ 6 (pI was determined using ExPASy tool).

The surface coverage Γ (in μg cm^{-2}) of PVX was estimated given the dimensions of PVX and its molecular weight; PVX is a flexible filament measuring 515 nm in length and 13 nm in diameter, its molecular weight lies at 35×10^6 g mol^{-1}, i.e., a single PVX weighs 6×10^{-17} g and occupies a surface area of ≈7000 nm^2. A closely packed monolayer of PVX would require 1.4×10^{10} particles with a weight of 830 ng. Therefore, experimentally we obtained a surface coverage of Γ 30% for native PVX and Γ 15% for PVX^{SpAB}CP. To assess the accuracy of the calculations based on changes in Δf, we performed atomic force microscopy measurements to image the surfaces upon PVX^{SpAB}CP immobilization (Figure 7). Indeed, AFM images were consistent with our calculations and indicated ≈20% surface coverage of the randomly adsorbed PVX^{SpAB}CP particles.

It is important to note the increased antibody (human total IgG) deposition on the PVX^{SpAB}CP-functionalized gold sensor chips—with a total mass change of Δm

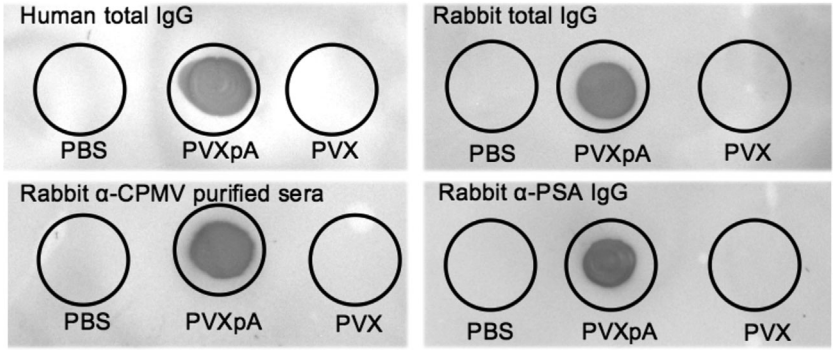

Figure 5. Dot blot tests probing antibody capture of PVX^{SpAB}CP. PBS, PVX^{SpAB}CP, or PVX were spotted onto nitrocellulose membranes and then probes with total human IgG, total rabbit IgG, rabbit anti-CPMV protein G purified serum, and rabbit anti-prostate specific antigen IgG antibodies followed by detection using anti-human or anti-rabbit alkaline phosphatase-labeled secondary antibodies. The dark signal indicates successful antibody immobilization.

$= 326.3$ ng; a single antibody has a molecular weight of 1.5×10^5 g mol^{-1} and dimensions of 5×7 nm. This would equate to approximately 500 antibodies per PVX^{SpAB}CP particle. While in closely packed confirmation, around 400 antibodies could occupy a half cylinder of PVX^{SpAB}CP immobilized on a surface, it is unlikely that this confirmation could be accomplished experimentally. It is possible that in addition to antibody captured by PVX^{SpAB}CP, some amount of antibody would account for antibody non-specifically adsorbed onto the gold sensor surface (see also values obtained for non- and PVX-coated gold sensor chips).

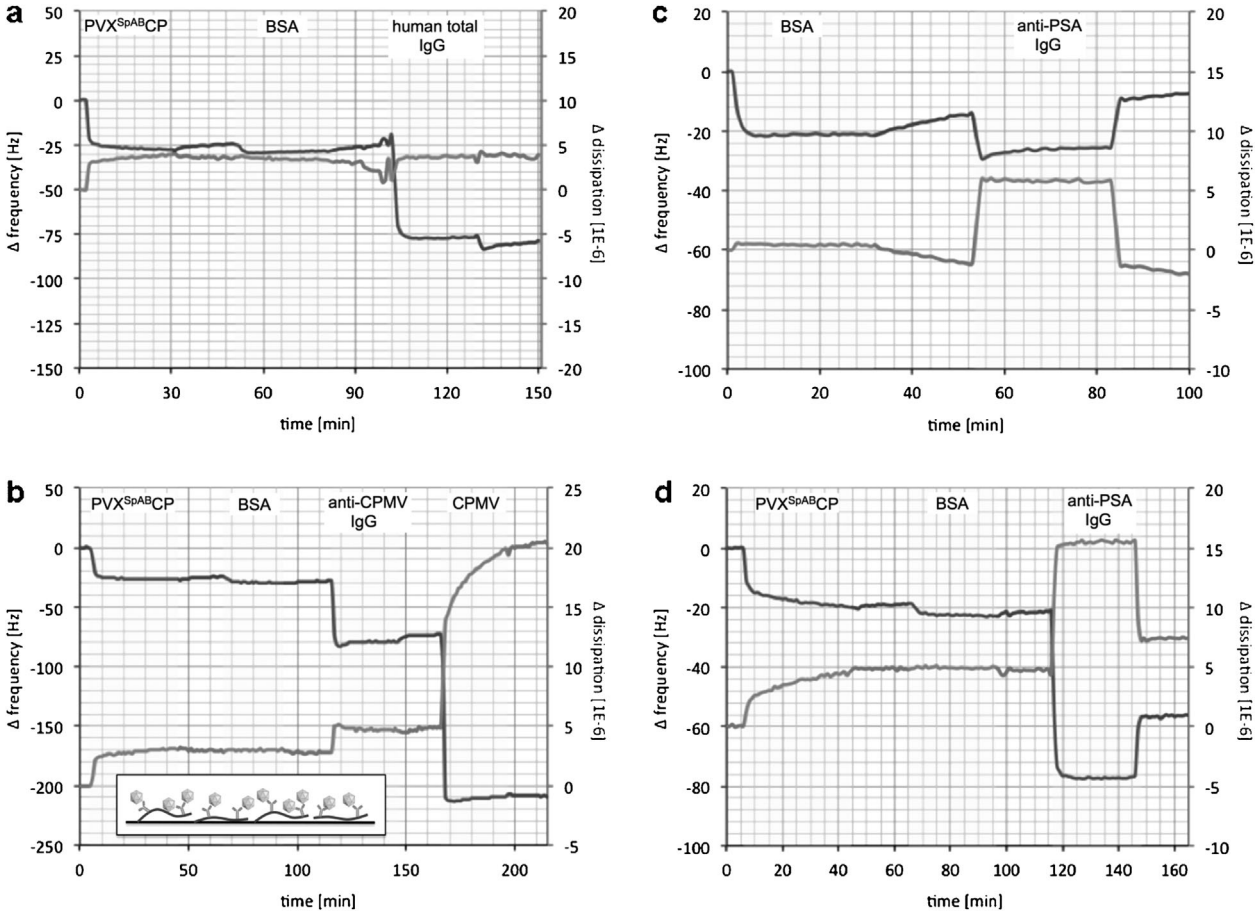

Figure 6. Antibody–PVX^{SpAB}CP interactions studied by quartz crystal microbalance with dissipation monitoring (QCM-D). PVX^{SpAB}CP was immobilized on a gold sensor chips and probed with human total IgG (a), rabbit anti-CPMV protein G purified serum (b), and rabbit anti-prostate specific antigen IgG antibodies (d); blocking was done using BSA. In control experiments, PVX^{SpAB}CP was omitted to monitor non-specific antibody adsorption (c) or native PVX was used (see Table 1). Changes in Δf and ΔD monitored by QCM-D are plotted against time; overtone $n = 1$, 3, 5, 7, 9, 11, and 13 were recorded, $n = 5$ is shown.

Table 1. Changes in Δf and ΔD monitored by QCM-D for the immobilized antibodies on PVX^{SpAB}CP-functionalized gold chip sensor surfaces and respective controls.

	Δf [Hz]	ΔD [1E-06]	Net Δm [ng]	Δf [Hz]	ΔD [1E-06]	Net Δm [ng]	Δf [Hz]	ΔD [1E-06]	Net Δm [ng]
Array	**PVX**			**Antibody**			**Analyte (CPMV)**		
Direct IgG immobilization	NA	NA	NA	−29.3	−0.8	172.7	NA	NA	NA
PVX–human total IgG	−50.3	14.8	296.7	−30.0	2.13	177.2	NA	NA	NA
PVX^{SpAB}CP–human total IgG	−26.8	4.7	158.4	−55.3	−0.2	326.3	NA	NA	NA
PVX^{SpAB}CP–aCPMV–CPMV	−27.3	4.1	161.1	−46.1	−0.7	273.1	−144.7	12.5	853.6
Direct aPSA immobilization	NA	NA	NA	9.9	8.7	−58.6	NA	NA	NA
PVX^{SpAB}CP–aPSA	−22.2	5.7	131.2	−34.5	10.9	204.1	NA	NA	NA

*Net Δm (ng) = mass deposited after washing

We extended the QCM-D studies to evaluate the immobilization of other antibodies, rabbit anti-PSA, and rabbit anti-CPMV antibodies were studied. Immobilization of rabbit anti-PSA antibodies directly onto the gold sensor surface was not accomplished; in fact the positive change in $\Delta f = 9.9$ Hz accompanied with significant changes in ΔD *of* $+7 \times 10^6$ indicates structural changes, such as reordering and loss of molecules, in the system. Data indicate that the rabbit anti-PSA antibodies indeed interact with the surface, but are entirely removed during the washing step—further it is indicated that additional losses are observed, which may indicate desorption of BSA blocking molecules through disorder in the system. In stark contrast, the PVX^{SpAB}CP-functionalized gold sensor enabled the capture of significant amount of rabbit anti-PSA antibodies. The recorded changes in frequency of $\Delta f = -345$ Hz correspond to change in mass of $\Delta m = 204.1$ ng; based on the surface coverage of PVX^{SpAB}CP this would equate to ≈300 antibodies captured per PVX. Anti-PSA antibody immobilization was also accompanied with changes in dissipation $\Delta D = 10.9 \times 10^6$, which is in agreement with loss of non-specifically adsorbed antibodies. Nevertheless, a significant amount of antibody is immobilized through engineered bio-specificity of the PVX^{SpAB}CP nanoparticles. Therefore, our PVX^{SpAB}CP chip sensor surfaces may be useful for the capture and immobilization of antibodies that are otherwise challenging to capture using non-specific adsorption. In particular, the anti-PSA antibody functional sensor chip surface may be a useful tool to aid prostate cancer diagnosis and prognosis.

Last but not least, we also demonstrated successful immobilization of anti-CPMV antibodies onto the PVX^{SpAB}CP-functionalized sensor chips. Stable immobilization of the anti-CPMV antibodies was apparent, with $\Delta f = -46.1$ Hz ($\Delta m = 273.1$ ng, which equates to ≈400 antibodies per PVX filament) and negligible changes in dissipation $\Delta f = -0.7 \times 10^{-17}$. Toward biosensing applications, we also tested whether the captured anti-CPMV antibodies would be functional in that they detect their analyte, cowpea mosaic virus (CPMV): indeed, sensitive detection of CPMV was achieved using the PVX^{SpAB}CP virus sensor (Table 1, Figure 6).

Overall, we found that antibodies purified from human and rabbit sera could be immobilized and captured using the PVX^{SpAB}CP filaments; in one example, we also demonstrated sensing capabilities. There was some variability

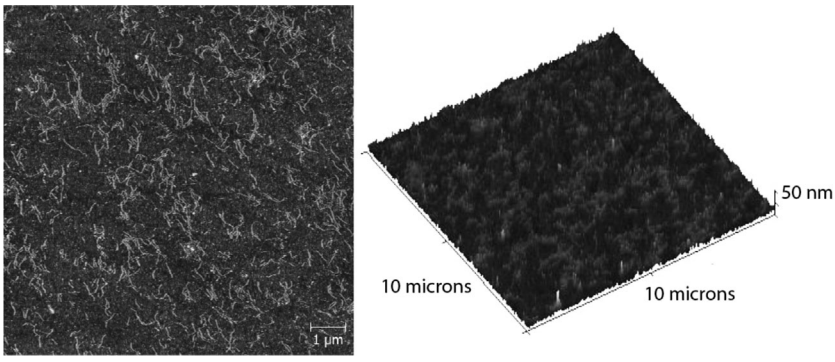

Figure 7. AFM imaging of PVX^{SpAB}CP bound onto QCM-D gold sensor chips. Surfaces were prepared using the QCM-D set up and analyzed in tapping mode by AFM; ImageJ software and surface subtraction tool were used to analyze the surface coverage; PVX^{SpAB}CP reached a surface coverage of 20%.

in antibody deposition, we found that between 300 and 500 antibodies were bound per PVX^{SpAB}CP filaments using anti-PSA, anti-CPMV, and total human IgG; this variability may be explained by varying non-specific absorption of the antibody formulations. For example, some degree of non-specific binding to the gold chips were observed using total human IgG (see above). Future investigations should set out to investigate the binding affinity and packing density on the filamentous PVX immunosorbent nanoparticles in more detail, to address whether differences occur comparing antibodies from different species. Furthermore, the biosensor assembly could be optimized through additional washing and blocking steps to avoid non-specific adsorption of antibodies or the analyte.

3. Conclusion

We report the development of immunoabsorbent nanoparticles based on the PVX platform technology. Three distinct genetic designs were chosen, all of which resulted in nanoparticles with protein A fragments displayed along the filamentous structure of the PVX backbone. It should be noted that this is the first report demonstrating the direct fusion of a 60 amino acid (aa) protein to the coat protein of PVX. This is an exciting development and opens the door for high-density protein display through genetic design for application in biotechnology and medicine.

Toward the implementation into devices, we demonstrate the application of PVX^{SpAB}CP in biosensing applications. In this application, we used quartz crystal microbalance and dissipation monitoring as an analytical platform; however, the technology could be combined with alternative read-outs such as optical or impedance measurements. Future studies will set out to further optimize the design to increase the density of PVX^{SpAB}CP bound to the gold sensor chips; maximizing antibody load and presentation is expected to yield highly sensitive sensors for applications in health and environmental monitoring. Increased loading could be accomplished through covalent deposition techniques; further, we will consider multilayered assemblies and configurations in which the particles are deposited standing-up on the surface to increase the overall surface area.

We envision broad application of the functionalized immunoabsorbent nanoparticles; for example, others suggested the use of protein A-displaying tobacco mosaic virus (TMV) particles as industrial immunoadsorbent for antibody purification.[21] Sensing applications could be broadly applied in the areas of medical and environmental sensing: for example, proposed sensors could be implemented for screening of disease biomarkers in patient samples. Alternatively, when combined with appropriate antibodies, the proposed sensors could find utility in the sensing of pathogens, toxins, or other hazards in specimens collected from patients, life stock, or drinking water. In addition to sensing applications, the arrays could function to capture pollutants for cleanup or detoxification. Furthermore, when combined with medical payloads—such as contrast agents or therapeutics, the chimeric PVX^{SpAB}CP could serve as a targeted nanoparticle technology in molecular imaging and drug delivery.

4. Materials and Methods

4.1. PVX Plasmid and Vector Constructs

Viral expression vectors used in this study are derived from the pCXI vector (kindly provided by Santa-Cruz, Horticulture Research International (HRI), East Malling, United Kingdom), containing a GFP-2A-CP fusion gene under the transcriptional control of the subgenomic CP promoter.[19] pCXI was modified by either replacing the 2A and GFP sequences or the GFP sequence only by the protein A sequence, resulting in the expression of the protein A sequence as direct in-frame translational CP fusion or as a fusion via the FMDV 2A coding sequence.[23,24] Furthermore, the protein A sequence was also cloned into the newly designed CXG4SI vector, which originates from the CXI vector, where the 2A sequence was replaced by a 15-aa linker peptide consisting of three repeats of the aa sequence Gly–Gly—Gly–Gly–Ser ($(G_4S)_3$).

The protein A sequence was amplified by PCR using the pGA4-protA vector as template (kindly provided by J. Lüddecke), which contains a truncated protein A sequence comprising 60 aa. Amplifications were carried out using primers EagIprotA and protABspEI for subsequent cloning into the pCXI and pCXG4SI vectors and for splice overlap extension (SOE) PCR[25] primer pairs protA3′cpSOEfor and universe and EagIprotA and protA3′rev were used. Primer ProtA3′rev is reverse complement to a part of the ProtA3′cpSOEfor primer, which contains 3′-protA and 5′-CP sequences. After separate production of these two PCR products, they were fused and amplified via SOE PCR using the external primers EagIprotA and universe.

Primers incorporated restriction sites suitable for cloning into pCXI and pCXG4SI (Table 2). Following amplification, the PCR products first were inserted into the pCR2.1 vector (Invitrogen), released using restriction enzymes *Eag*I and *Bsp*EI or *Stu*I as appropriate, and inserted into the CXI or CXG4SI vector, which had been linearized using the same enzymes to produce recombinant vectors pPVX^{SpAB}CP, pPVX$^{SpAB\text{-}2A}$CP, and pPVX$^{SpAB\text{-}G4S}$CP, respectively. Plasmid DNA used for plant infection was amplified in the general *Escherichia coli* cloning strain DH5α.

Table 2. Primer sequences.

Primer name	Nucleotide sequence (5′-3′)
BspEIGGGGScp	5′-ATCCGGAGGTGGAGGTAGCGGCGGTGGAGGGAGTGGTGGAGGCGGTAGCCCCG CGAGCACAACACAGC-3′
EagIProtA	5′-ACGGCCGATGGCTGCAGACAACAAGTTCAACAAGG-3′
ProtABspEI	5′-ATCCGGACTTTGGTGCTTGAGCATC-3′
ProtA3′cpSOEfor	5′-GATGCTCAAGCACCAAAGCCCGCGAGCACAACACAGC-3′
ProtA3′rev	5′-CTTTGGTGCTTGAGCATC-3′
CX1	5′-TTGAAGAAGTCGAATGCAGC-3′
CX2	5′-CTAGATGCAGAAACCATAAG-3′
CX3	5′-ATAGCAGTCATTAGCACTTC-3′
CX4	5′-CGGGCTGTACTAAAGAAATC-3′

4.2. Immunocapture RT-PCR and Sequencing

0.5 ml tubes were coated with 100 μl PVX pAb (1:100 in coating buffer) over night at 4 °C. After three times wash with 500 μl PBST buffer each, the coated tubes were incubated with 100 μl plant sap (1:20 diluted with PBS) for 2 h at 37 °C. For cDNA synthethis the QIAGEN OneStep RT-PCR Kit was used as described by the manufacturer (Qiagen). Resulting cDNA was then amplified using Taq polymerase. Sequencing was performed using an ABI Prism 3700 DNA Analyzer (Applied Biosystems), primers CX2, CX3, or CX4 (Table 1) and the ABI Prism BigDye Terminator v3.0 Ready Reaction Cycle Sequencing Kit (Applied Biosystems).

4.3. PVX Propagation Through Farming in Plants

N. benthamiana plants were inoculated with plasmid pPVX201 (a kind gift from D. Baulcombe, The Sainsbury Laboratory, Norwich, United Kingdom) which carries the wild-type PVX CP gene.[26] Further inoculations were carried out with the protein A sequences containing plasmids pPVX^{SpAB}CP, pPVX$^{SpAB\text{-}2A}$CP, and pPVX$^{SpAB\text{-}G4S}$CP (Figure 1). Inoculation was achieved by gentle abrasion of the surfaces of three leaves per plant with Celite 545 (Roth) and 10 μg of plasmid DNA. 10 min post inoculation, the surface of the leaves was rinsed with tap water in order to remove Celite and excess DNA. Plants were maintained with a 16-h photoperiod (25 000–30 000 lux, 25 °C/20 °C temperature regime) and 60% humidity. Upon full systemic infection (≈14 d post infection) fusion protein expression was confirmed by western blot and electron microscopy; then scaled-up production was initiated.

4.4. PVX Purification

PVX particles were purified according to a modified PVX purification protocol (http://www.cipotato.org/training/Materials/PVTechs/Fasc5.2(99).pdf) from CIP (International Potato Center, Lima, Peru), which is based on PEG precipitation and sucrose gradient centrifugation. Briefly, 100 g of systemically infected leave material stored at −80 °C was homogenized in two volumes of ice-cold 0.1 M phosphate buffer (pH 8.0) containing 10% ethanol. After filtration through three layers of gauze, the mixture was supplemented with (v/v) 0.2% 2-mercaptoethanol. Cellular debris was removed by centrifugation (7800*g*, 20 min, 4 °C) and the supernatant was supplemented with 1% Triton X-100. The solution was stirred for 1 h at 4 °C and clarified by centrifugation (5500*g*, 20 min, 4 °C). The supernatant was processed for precipitation with 0.2 M NaCl and 4% (w/v) PEG, stirred for 1 h at 4 °C and for 1 h at room temperature. Virus particles were precipitated by centrifugation (7800*g*, 30 min, 4 °C) and resuspended in 4 ml 0.05 M phosphate buffer (pH 8.0) with 1% (v/v) of Triton X-100. The solution was clarified (7800*g*, 10 min, 4 °C) and the supernatant was loaded onto a 10–45% (14 ml each) sucrose gradient in 0.01 M phosphate buffer (pH 7.2) containing 0.01 M EDTA. After 75 min centrifugation (104 000*g* 4 °C), fractions were collected from the bottom in 1.5 ml steps. Sucrose gradient fractions containing PVX particles, as verified by sodium dodecylsulfate polyacrylamide gel electrophoresis (SDS-PAGE), were combined, filled up to 10 volumes with 0.01 M phosphate buffer (pH 7.2) and centrifuged (248 000*g*, 4 °C, 3 h). The pellets were dissolved by continuous stirring in 2 ml 0.01 M phosphate buffer (pH 7.2) overnight. After clarification by centrifugation at 5000*g*, 10 min, 4 °C, the concentration of virus was calculated using the PVX extinction coefficient (2.97) for the extinction values at 260 nm.

4.5. SDS-PAGE and Western Blot Analysis

The protein profiles of crude sap extracts (1:3 dilution) or purified virus preparations were analyzed by SDS-PAGE using a 12% resolving gel and a 4% stacking gel, after

samples had been incubated at 100 °C for 5 min in loading buffer.[27] The separated proteins were transferred onto Hybond-C transfer membranes (Amersham) using the Mini Trans-Blot Cell (BioRad). Western blot analysis was performed using PVX polyclonal antibodies (DSMZ, Braunschweig, Germany), as primary antibodies and alkaline phosphatase (AP)-conjugated goat anti-rabbit (GAR) IgG (Dianova) as secondary antibodies.

4.6. Electron Microscopy

Electron microscope grids with a Pioloform-carbon support film were floated for 15 min on drops of virus-infected plant sap diluted 1:3 with PBS or on purified virus preparation (10 μg), washed once with 20 drops of PBS containing 0.05% Tween-20 (PBST) and blocked with 0.1% bovine serum albumin (BSA; Sigma) in phosphate buffer (pH 7.2). Gold labeled antibodies (15-nm gold particles (Biocell, United Kingdom)) were bound to the sample by incubating the grid with the appropriate antibody diluted in PBST for at least 90 min or overnight. The grids were washed extensively (twice with PBST, twice with distilled H_2O) and the samples were stained with five drops of 1% uranyl acetate. Electron microscopy was carried out using a Zeiss EM 10 (Institute for Zoology, RWTH-Aachen).

4.7. Dot Blots

Dot blot tests were performed to evaluate antibody–PVX^{SpAB}CP specificity using total human IgG (Sigma–Aldrich), total rabbit total IgG (Sigma–Aldrich), rabbit anti-CPMV protein G purified serum (sera were obtained from Pacific Immunology), and rabbit anti-prostate specific antigen IgG (PSA, EMD Millipore). 2 μL of PBS, PVX, and PVX^{SpAB}CP (at 0.05 mg mL^{-1}) was spotted onto a nitrocellulose membrane and the solution was allowed to dry. Membranes were blocked using 5% (w/v) milk in Tris-buffered Saline with 0.02% (v/v) Tween (TBST) and incubated overnight at 4 °C on a plate rocker. Membranes were washed three times with TBST prior to addition of the test antibodies (total human IgG, total rabbit IgG, rabbit anti-CPMV protein G purified serum, and rabbit anti-prostate specific antigen IgG) at a 1:500 dilution in 5% (w/v) milk in TBST solution; the membranes were incubated for 1 h at room temperature and then washed six times with TBST. For detection, a secondary antibody, alkaline phosphatase-labeled
anti-human or anti-rabbit IgG, was introduced using a 1:500 dilution in 5% (w/v) in TBST solution for 1 h at room temperature and then washed six times with TBST. Staining of the membrane paper was performed using NBT/BCIP solution (Sigma–Aldrich), procedures were according to the manufacturer's instructions. Staining was allowed to occur until a significant color change was detectable or for a maximum of 20 min; then membranes were washed with deionized water and a photograph was taken under white light.

4.8. Quartz Crystal Microbalance With Dissipation Monitoring (QCM-D)

Antibody-to-PVX^{SpAB}CP binding and subsequent sensing capabilities were evaluated using a Q-Sense quartz crystal microbalance with dissipation monitoring (QCM-D) with gold sensor chips (Biolin Scientific). After verification of temperature control at 25 °C, overtones of the frequencies used, and average initial dissipation recorded for each overtone, the sensor chip was primed first using deionized water, and then equilibrated to the running buffer of 10 mM potassium phosphate (pH 7.4) at flow conditions of 150 μL min^{-1} for 15 min each. All subsequent samples were analyzed using running buffer. Samples were injected at 150 μL min^{-1} for 5 min to ensure particle presence in the flow chamber, followed by incubation on the surface of the sensor chip under static conditions (0 μL min^{-1}) for 25 min to allow for maximum deposition and coverage of the chip. Excess particles were then removed via a wash cycle using running buffer at 150 μL min^{-1} for 20 min. For the experimental data sets, PVX or PVX^{SpAB}CP (at 1 mg mL^{-1}) were injected first, followed by a blocking step using 10% (w/v) bovine serum albumin (BSA, Sigma–Aldrich) in running buffer, then antibodies of interest (total human IgG, rabbit anti-CPMV protein G purified serum, and rabbit anti-prostate specific antigen IgG) were injected at concentration of 1 mg mL^{-1} in running buffer. To test for sensing capabilities, we also subjected the PVX^{SpAB}CP-immobilized anti-CPMV chip to purified CPMV (at 1 mg mL^{-1}). For controls, experiments were repeated omitting the PVX^{SpAB}CP immobilization step.

4.9. Atomic Force Microscopy (AFM) Imaging

Immobilization of PVX^{SpAB}CP particles on QCM-D sensor surfaces was verified using a PicoScan 2500 (Agilent Technologies formerly Molecular Imaging) atomic force microscope in tapping mode. The instrument is equipped with a piezo scanner capable of imaging 10 μm × 10 μm sample areas at room temperature and commercially available tapping mode tips (NSG30, K-TEK Nanotechnology). These AFM tips have a gold reflective side, a resonant frequency within 240–440 kHz, and a force constant of 40 N m^{-1}. All tapping mode AFM images were scanned at 0.65–1.05 Hz. Gwyddion 2.19 was then used to flatten and filter the topographic AFM images.

Acknowledgements: This work was supported in parts by a grant from the National Science Foundation CMMI 1333651 (to N.F.S. and R.C.A.) and DMR 1452257 (to N.F.S.).

Received: July 26, 2015; Revised: August 30, 2015; Published online: October 6, 2015; DOI: 10.1002/mabi.201500280

[1] R. Danczyk, B. Krieder, A. North, T. Webster, H. HogenEsch, A. Rundell, *Biotechnol. Bioeng.* **2003**, *84*, 215.
[2] P. Carter, *Nat. Rev. Cancer* **2001**, *1*, 118.
[3] P. D. Senter, *Current Opin. Chem. Biol.* **2009**, *13*, 235.
[4] M. Arruebo, M. Valladares, Á. *González-Fernández, J. Nanomater.* **2009**, 2009, 1.
[5] S. H. Brewer, W. R. Glomm, M. C. Johnson, M. K. Knag, S. Franzen, *Langmuir* **2005**, *21*, 9303.
[6] R. Koenig, D. E. Lesemann, *Potato Virus X, Potexvirus Group*, A. F. Murant, B. D. Harrison, Eds., Warwick: Association of Applied Biologists **1989**, p. 1.
[7] C. Lico, C. Mancini, P. Italiani, C. Betti, D. Boraschi, E. Benvenuto, S. Baschieri, *Vaccine* **2009**, *27*, 5069.
[8] C. Marusic, P. Rizza, L. Lattanzi, C. Mancini, M. Spada, F. Belardelli, E. Benvenuto, I. Capone, *J. Virol.* **2001**, *75*, 8434.
[9] K. Uhde-Holzem, V. Schlosser, S. Viazov, R. Fischer, U. Commandeur, *J. Virol. Methods* **2010**, *166*, 12.
[10] N. Cerovska, H. Hoffmeisterova, T. Moravec, H. Plchova, J. Folwarczna, H. Synkova, H. Ryslava, V. Ludvikova, M. Smahel, *J. Biosci.* **2012**, *37*, 125.
[11] H. Plchova, T. Moravec, H. Hoffmeisterova, J. Folwarczna, N. Cerovska, *Protein Expr. Purif.* **2011**, *77*, 146.
[12] P. L. Chariou, K. L. Lee, A. M. Wen, N. M. Gulati, P. L. Stewart, N. F. Steinmetz, *Bioconjug. Chem.* **2015**, *26*, 262.
[13] K. L. Lee, S. Shukla, M. Wu, N. R. Ayat, C. E. El Sanadi, A. M. Wen, J. F. Edelbrock, J. K. Pokorski, U. Commandeur, G. R. Dubyak, N. F. Steinmetz, *Acta Biomater.* **2015**, *19*, 166.
[14] S. Shukla, A. L. Ablack, A. M. Wen, K. L. Lee, J. D. Lewis, N. F. Steinmetz, *Mol. Pharm.* **2013**, *10*, 33.
[15] N. F. Steinmetz, M. E. Mertens, R. E. Taurog, J. E. Johnson, U. Commandeur, R. Fischer, et al. *Nano Lett.* **2010**, *10*, 305.
[16] K. Uhde-Holzem, R. Fischer, U. Commandeur, *Arch. Virol.* **2007**, *152*, 805.
[17] N. Carette, H. Engelkamp, E. Akpa, S. J. Pierre, N. R. Cameron, P. C. Christianen, et al. *Nat. Nanotechnol.* **2007**, *2*, 226.
[18] W. L. Hoffman, D. J. O'Shannessy, *J. Immunol. Methods* **1988**, *112*, 113.
[19] S. S. Cruz, S. Chapman, A. G. Roberts, I. M. Roberts, D. A. Prior, K. J. Oparka, *Proc. Natl. Acad. Sci. U S A* **1996**, *93*, 6286.
[20] J. Goudswaard, J. A. van der Donk, A. Noordzij, R. H. van Dam, J. P. Vaerman, *Scand. J. Immunol.* **1978**, *8*, 21.
[21] S. Werner, S. Marillonnet, G. Hause, V. Klimyuk, Y. Gleba, *Proc. Natl. Acad. Sci. U S A* **2006**, *103*, 17678.
[22] G. Sauerbrey, *Zeitschrift für Physik.* **1959**, *155*, 206.
[23] M. D. Ryan, J. Drew, *Embo J.* **1994**, *13*, 928.
[24] M. D. Ryan, A. M. King, G. P. Thomas, *J. Gen. Virol.* **1991**, *72*, 2727.
[25] A. N. Warrens, M. D. Jones, R. I. Lechler, *Gene* **1997**, *186*, 29.
[26] D. C. Baulcombe, S. Chapman, S. Santa Cruz, *Plant J.* **1995**, *7*, 1045.
[27] UK Laemmli, *Nature* **1970**, *227*, 680.